JOURNAL OF MATERIALS SCIENCE **33** (1998) 4727–4732

Fracture behaviour of boride-dispersed composites fabricated by hot-pressing amorphous $Ni_{60}Mo_{30}B_{10}$ powder

I. J. DAVIES, A. NOZUE, S. NAKABAYASHI, T. OKUBO
Department of Mechanical Engineering, Sophia University, Tokyo, Japan
E-mail: a-nozue@me.sophia.ac.jp

Microstructural and mechanical property characteristics were investigated for three boride-dispersed composites fabricated by hot-pressing amorphous $Ni_{60}Mo_{30}B_{10}$ powder. The first composite was tested in the as-hot-pressed condition (HP) whilst the other specimens were subjected to a solution treatment (ST) and further ageing (STA). X-ray diffraction showed the HP and ST composites to consist of Mo_2NiB_2 particles in a Ni-rich matrix whilst the STA material contained Mo_2NiB_2 particles in a Ni_3Mo matrix. The hardness and fracture toughness decreased and increased, respectively, for the ST material compared to the HP case whilst the STA case showed increased and decreased hardness and fracture toughness, respectively, compared to the ST composite. These results were explained in terms of the brittle–ductile–brittle fracture modes for the HP–ST–STA specimens. In addition, the HP specimen showed only a 15% decrease in compressive strength at 973 K compared to 303 K.

1. Introduction

The application of nickel-based alloys to injection or extrusion of plastics requires high corrosion and wear resistance at elevated temperature [1]. Although molybdenum is known to be an effective suppressor of corrosion [2], particularly against sulphide [3] and halide [1] gases, Ni–Mo alloys possess low ductility (typically 5%) [4] as a result of long-range ordering [5, 6] of Ni_4Mo at grain boundaries [7–9]. Improved ductility may be achieved through addition of boron [4, 10, 11] which decreases discontinuous ordering at the grain boundaries and changes the fracture mode from intergranular to transgranular. In addition, improved wear resistance may result [1] through the formation of hard boride phases. However, effective utilization of boron has been limited by its low solid solubility in these alloys [12].

In order to overcome this problem, amorphous Ni–Mo–B alloys have been developed [12–15] which have the advantage of improved homogeneity and provide a wider range of solute content compared to normal manufacturing routes. These alloys are produced in the form of thin ribbons (25–50 μm thick) [13] using ultra-rapid solidification at rates greater than $10^6\,^\circ C\,s^{-1}$ whilst consolidation normally involves hot pressing, extrusion, or dynamic consolidation [13, 16]. Such a manufacturing process also results in a low oxygen content [13], which is advantageous for reducing embrittlement [11]. The resulting alloys, following suitable heat treatment [15], possess good hardness, wear, and corrosion resistance at elevated temperature [13] with applications including dies and tools. However, despite showing superior mechanical properties and corrosion resistance compared to previous alloys, data on amorphous Ni–Mo–B alloys is still fairly limited [13–22]. The aim of the present work was to investigate the effect of microstructure on the fracture characteristics of boride-dispersed composites fabricated by hot-pressing amorphous $Ni_{60}Mo_{30}B_{10}$ powder.

2. Experimental procedure

The starting powder for the alloys investigated in this work is amorphous $Ni_{60}Mo_{30}B_{10}$ (Ni–44.2%Mo–1.7%B (wt. %)) (Devitrium 3065, Allied Corporation) which possessed a characteristic platelet morphology from the production route [13] and is shown in Fig. 1. The amorphous nature of the powder may be inferred from the broad Ni (1 1 1) peak determined by X-ray diffraction (XRD) and is shown in Fig. 2.

The powder was consolidated in vacuum by using the hot pressing technique, a graphite die of 25 mm diameter, and the processing conditions indicated in Fig. 3; this specimen was referred to as "HP". Further specimens were solution treated (ST) in air at 1373 K for 1 h and followed by an optional ageing treatment (STA) for 4 h at 1373 K in air.

Chemical phases present within the three alloys were determined for polished specimens by using XRD (Shimazu XD-D1) and monochromatic CuK_α radiation (30 kV, 30 mA). The scanning range of 2Θ was 20–80° at a speed of $2^\circ\,min^{-1}$ whilst phases were identified with JCPDS data [23]. The hardness, H_v, of specimens was determined at room temperature by the micro-Vickers

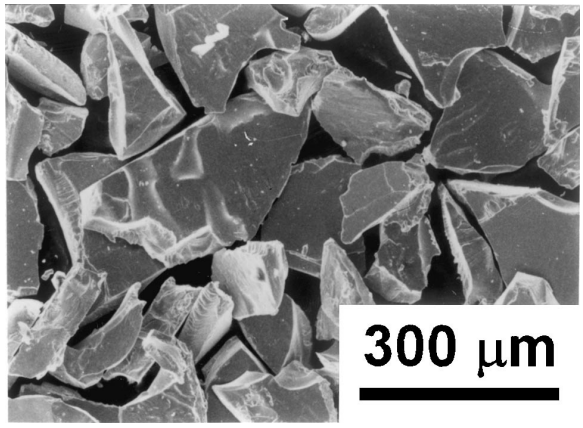

Figure 1 Scanning electron micrograph of amorphous $Ni_{60}Mo_{30}B_{10}$ powder.

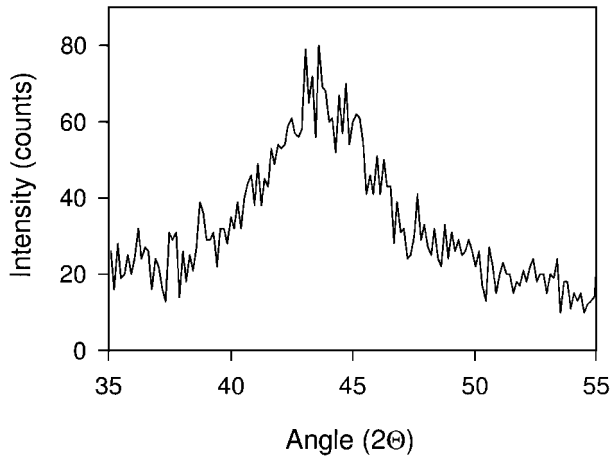

Figure 2 X-ray diffraction spectrum of amorphous $Ni_{60}Mo_{30}B_{10}$ powder.

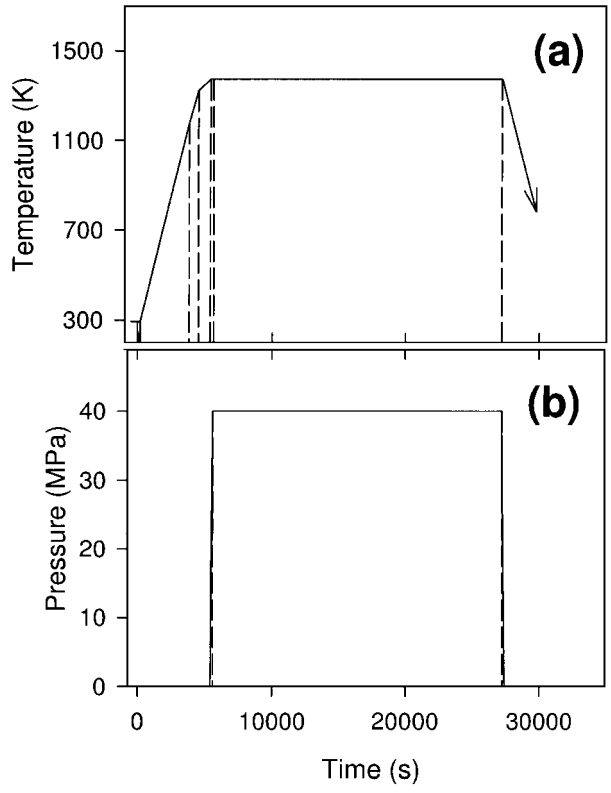

Figure 3 Hot pressing conditions for boride-dispersed composites produced from amorphous $Ni_{60}Mo_{30}B_{10}$ powder.

indentation technique (Akashi) on polished specimens with a load, F, of 4.9 N and loading time of 15 s. A minimum of 12 measurements were obtained for each specimen with the hardness being determined from

$$H_v = \frac{1854F}{d^2} \tag{1}$$

where d is the diagonal length of the indent.

The microstructure of specimens was determined with a Jeol JSM-6100 scanning electron microscope (SEM) at 25 kV following etching for 5–10 s in a solution of 40 ml HCl, 10 ml HNO_3, 2.5 g $FeCl_3$, and 2.5 g $CuCl_2$.

The fracture toughness, K_{IC}, of specimens at room temperature was measured with the compact tension (CT) configuration whilst specimen dimensions have been indicated in Fig. 4a. A clip gauge was used to measure the crack opening displacement (COD) with fracture toughness being determined from the COD versus load curve at 5% offset using

$$K_{IC} = \frac{F}{bw^{1/2}}\left(2+\frac{a}{w}\right)\left\{0.76+4.8\frac{a}{w}-11.58\left(\frac{a}{w}\right)^2 + 11.43\left(\frac{a}{w}\right)^3-4.08\left(\frac{a}{w}\right)^4\right\}\left(1-\frac{a}{w}\right)^{-3/2} \tag{2}$$

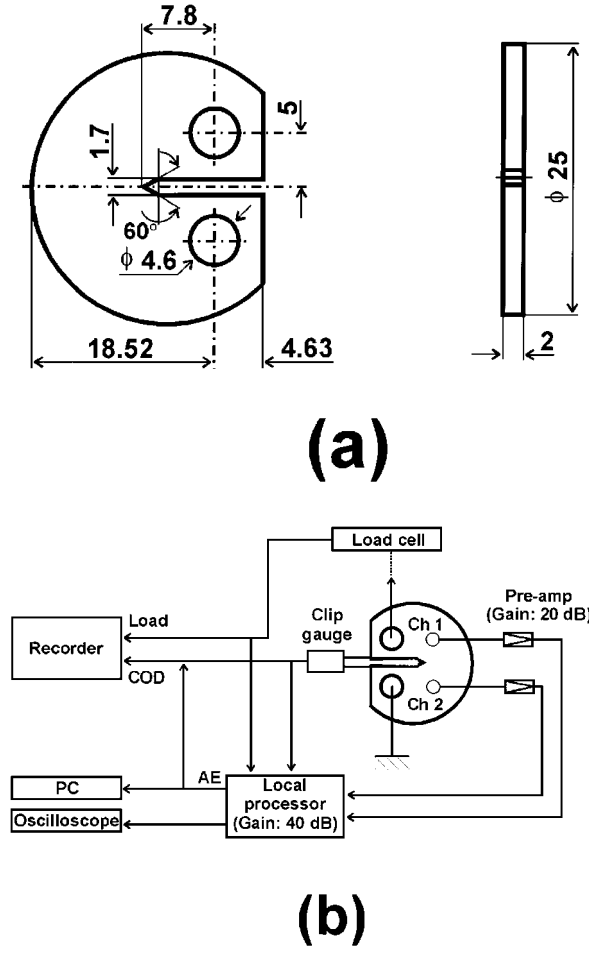

Figure 4 Schematic representation of: (a) fracture toughness specimen, and (b) fracture toughness apparatus.

where b is the specimen thickness, a is the crack length, and w is the distance from load point to external diameter of the specimen. The crack path during fracture toughness tests was observed *in situ* with an SEM equipped with a servo-controlled loading apparatus. Acoustic emission (AE) was measured simultaneously during the fracture toughness experiment with the configuration detailed in Fig. 4b. AE sensors with a 300 kHz resonant frequency were fixed to the specimen by electron wax and events were detected with a two-channel AE apparatus after 40 dB preamplification. The threshold voltage for detection was 100 mV (equivalent to 40 dB) with a time resolution of 0.125 μs.

The compressive properties of specimens were determined at 303, 773 and 973 K with specimen dimensions of $2.5 \times 2.5 \times 4$ mm and a strain rate of 2.1×10^{-3} s^{-1}. The 0.2% proof strength, compressive strength, and strain to failure were determined for all test conditions employed.

3. Results and discussion

Scanning electron micrographs of the HP, ST, and STA specimens are presented in Fig. 5 whilst the respective XRD spectra are shown in Fig. 6. All of the micrographs show equiaxed precipitated particles in a uniform matrix with a slight increase in particle size and numbers being observed for the ST and STA alloys. The XRD spectrum of the HP specimen shown in Fig. 6a indicated the microstructure (Fig. 5a) to consist of Mo_2NiB_2 precipitates in a Ni-rich matrix. Although the presence of Mo_2NiB_2 precipitate is in good agreement with the previous work [13, 17, 21, 22], there was no indication of Ni_3Mo and Ni_4Mo phases suggested by previous researchers to form in this alloy after hot-pressing under similar conditions [13, 19]. The lack of ordered Ni_3Mo and Ni_4Mo phases suggests rapid cool-down of the hot-press unit [13] and also that superior mechanical properties might be expected [13]. A similar XRD spectrum was observed for the ST specimens (Fig. 6b) although it was expected from the previous work [13, 15, 22] that an additional dispersion of very fine boride particles should be present within the matrix (Fig. 5b). However, this contribution to the XRD spectrum may have been obscured by that from the much larger Mo_2NiB_2 particles. The XRD spectrum of the STA alloy was considerably different from the HP and ST cases with transformation of the Ni matrix to an ordered Ni_3Mo phase having occurred.

It was stated previously for similar alloys [13] that formation of Ni_3Mo increased the alloy hardness but decreased ductility. Indeed, it can be seen from the hardness data presented in Table I that the STA alloy did exhibit the highest hardness and directly attributable to the presence of the Ni_3Mo. The decrease in hardness from HP to ST was consistent with that observed in earlier work by the authors [17] where it was attributed to dissolution of Mo_2NiB_2 particles in the matrix.

The COD versus load data obtained during the fracture toughness testing has been presented in Fig. 7 together with cumulative AE events, whilst micrographs illustrating crack paths and fracture surfaces for the three specimens are shown in Figs 8 and 9, respectively.

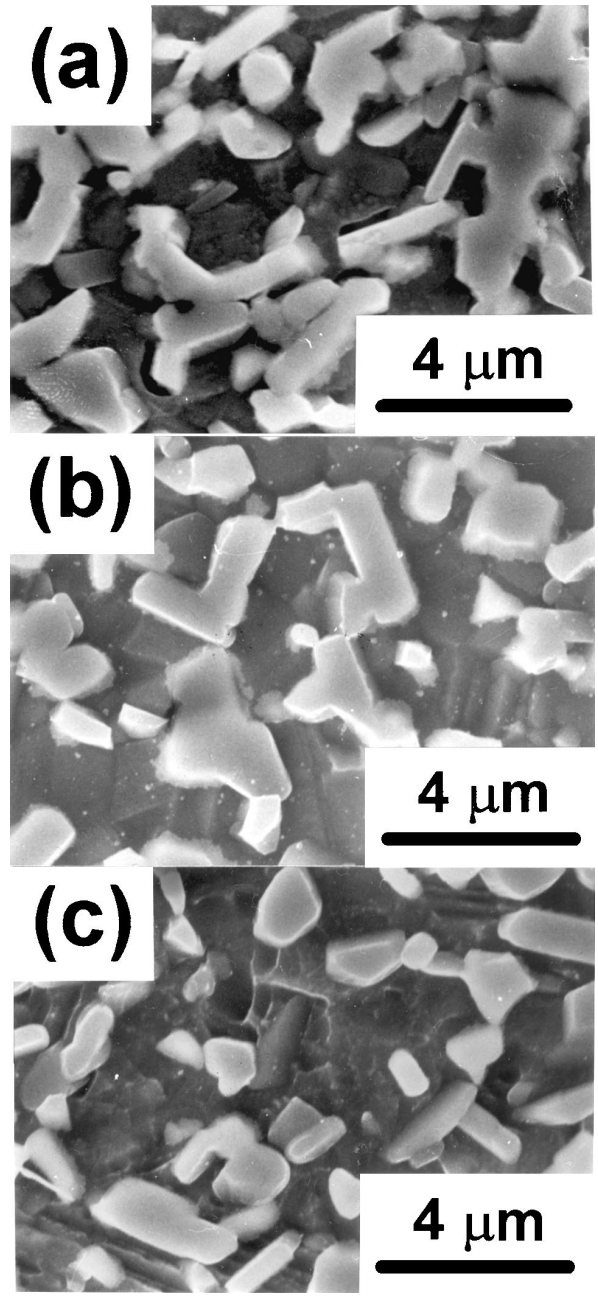

Figure 5 Scanning electron micrographs of boride-dispersed composites produced from amorphous $Ni_{60}Mo_{30}B_{10}$ powder: (a) HP, (b) ST, and (c) STA. HP, ST, and STA refer to materials hot-pressed, solution-treated after hot pressing, and solution-treated and aged, respectively.

Loading of the HP alloy in Fig. 7a showed a linear increase in COD until approximately 300 N where AE events in significant quantity were first observed. The number of AE events increased rapidly near the point of maximum load at approximately 450 N. Such a rapid increase in AE events would be indicative of fairly brittle behaviour as was confirmed from the fracture surface in Fig. 9a. The crack propagation followed an almost linear path as shown in Fig. 8a, although the failure was intergranular so that increased toughening due to the Mo_2NiB_2 particles was not thought significant; K_{IC} for the HP alloy was 14.6 MPa m$^{1/2}$.

Failure characteristics for the ST alloy were significantly different compared to that observed for the HP case. For the ST case indicated in Fig. 7b, AE events increased gradually until a load of ≈ 100 N whereupon the number of AE events increased sharply until the

TABLE I Summary of mechanical properties for boride-dispersed composites produced from amorphous $Ni_{60}Mo_{30}B_{10}$ powder

Properties		Temp. (K)	Heat treatment HP	ST	STA
Microstructure	Based phase		Ni		Ni_3Mo
	Particles			Mo_2NiB_2	
Hardness (H_v)	Compressive specimen		870	680	917
	CT specimen		769	635	861
		303	2.39	1.63	2.66
	0.2% proof strength (GPa)	773	2.15	1.49	2.56
		973	2.03	1.53	2.28
Strength	Compressive strength (GPa)	303	2.96	2.61	3.60
		773	2.56	2.39	2.94
		973	2.54	2.48	2.93
	Plastic deformation,	303	8.0	21.7	5.9
	compressive strain (%)	773	4.54	11.3	3.45
		973	7.84	14.0	10.6
Fracture toughness K_{IC} (MPa $m^{1/2}$)			14.6	22.8	11.3

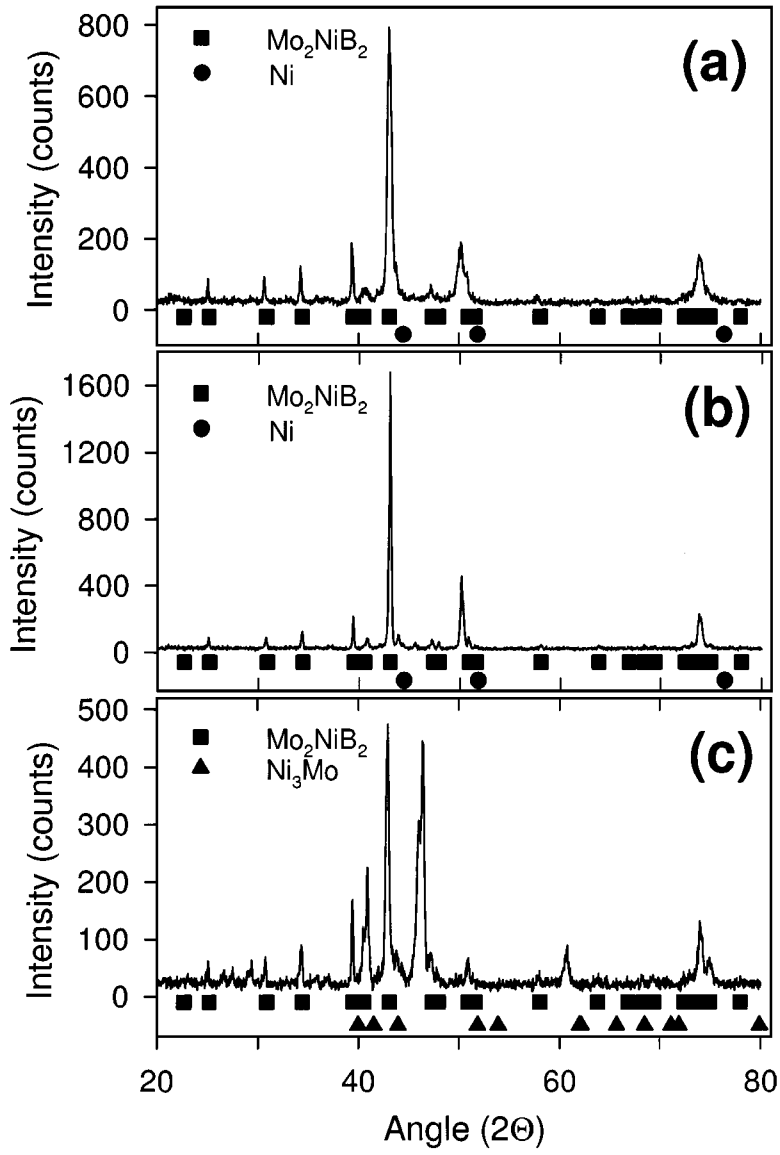

Figure 6 X-ray diffraction spectra of boride-dispersed composites produced from amorphous $Ni_{60}Mo_{30}B_{10}$ powder: (a) HP, (b) ST, and (c) STA.

maximum load of nearly 700 N. The increased maximum load and COD for the ST alloy, compared to the HP alloy, contributed to improved toughness for this alloy (22.8 MPa $m^{1/2}$) together with a fracture surface showing ductile characteristics as shown in Fig. 9b. This increase in fracture toughness showed itself in the fracture behaviour indicated in Fig. 8b with the crack path noted to be highly non-linear as a result of the slightly larger Mo_2NiB_2 particle size, compared to the HP alloy, and intergranular failure mode.

Although the STA alloy showed a small number of AE events below the maximum force of approximately

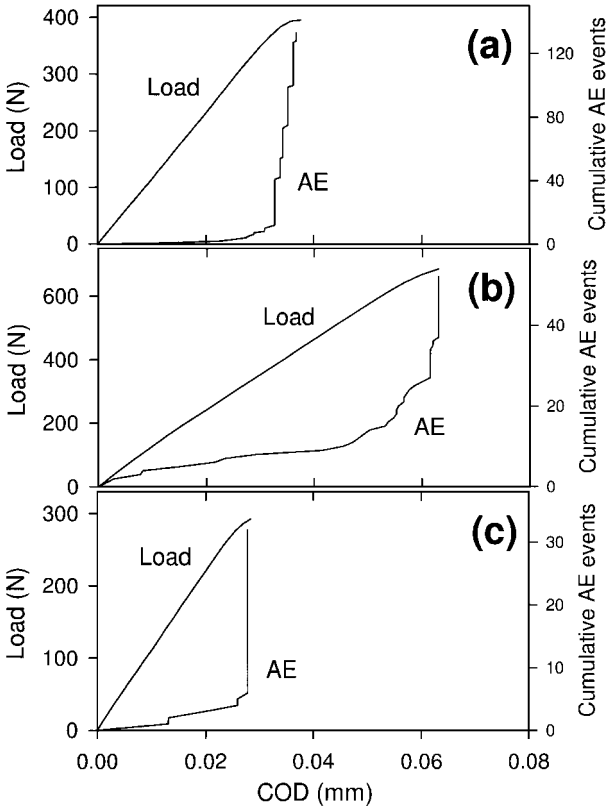

Figure 7 Load and cumulative acoustic emission events versus crack opening displacement for boride-dispersed composites produced from amorphous $Ni_{60}Mo_{30}B_{10}$ powder: (a) HP, (b) ST, and (c) STA.

33 N (Fig. 7c), nearly all events were concentrated at the point of maximum force. Such an AE event profile is characteristic of brittle failure as was confirmed by the lower maximum COD and force values compared to the HP and ST alloys, together with the fracture surface characteristics shown in Fig. 9c. In addition, the crack path for the STA alloy showed only minor deviation from linearity with a largely intergranular fracture mode and, as such, the fracture toughness of 11.3 MPa $m^{1/2}$ was significantly less than the STA alloy (22.8 MPa $m^{1/2}$) and similar to that of the HP case (14.6 MPa $m^{1/2}$). The poor fracture toughness of the STA alloy was mainly attributed to the brittle Ni_3Mo matrix [13].

Compressive stress/strain curves for the HP alloy at 303, 773 and 973 K have been presented in Fig. 10a whilst the comparison between HP, ST, and STA alloys at 303 K is indicated in Fig. 10b. From Fig. 10a it can be seen that compressive stress/strain paths for the HP alloy were similar in the elastic region for all cases whilst the compressive strength at 973 K was approximately 15% lower than that at 303 K, i.e. mechanical properties for the HP alloy were only slightly degraded at 973 K compared to those at 303 K, which is of importance for many applications [13]. The difference in failure strain at 773 K compared to that at 303 and 973 K was attributed to the change in microstructure between these temperatures.

4. Summary

Microstructural and mechanical property characteristics were investigated for three boride-dispersed composites fabricated by hot-pressing amorphous $Ni_{60}Mo_{30}B_{10}$ powder. The first composite was tested in the as-hot-pressing condition (HP) whilst the other specimens were subjected to a solution treatment (ST) and further ageing (STA). X-ray diffraction showed the HP and ST composites to consist of Mo_2NiB_2 particles in a Ni-rich matrix whilst the STA material contained Mo_2NiB_2 particles in a Ni_3Mo matrix. The hardness and fracture toughness decreased and increased, respectively, for the ST material compared to the HP case whilst the STA case showed increased and decreased hardness and fracture toughness, respectively, compared to the ST composite. These results were explained in terms of the brittle-ductile-brittle fracture modes for the HP–ST–STA specimens. In addition, the HP specimen showed only a 15% decrease in compressive strength at 973 K compared to 303 K.

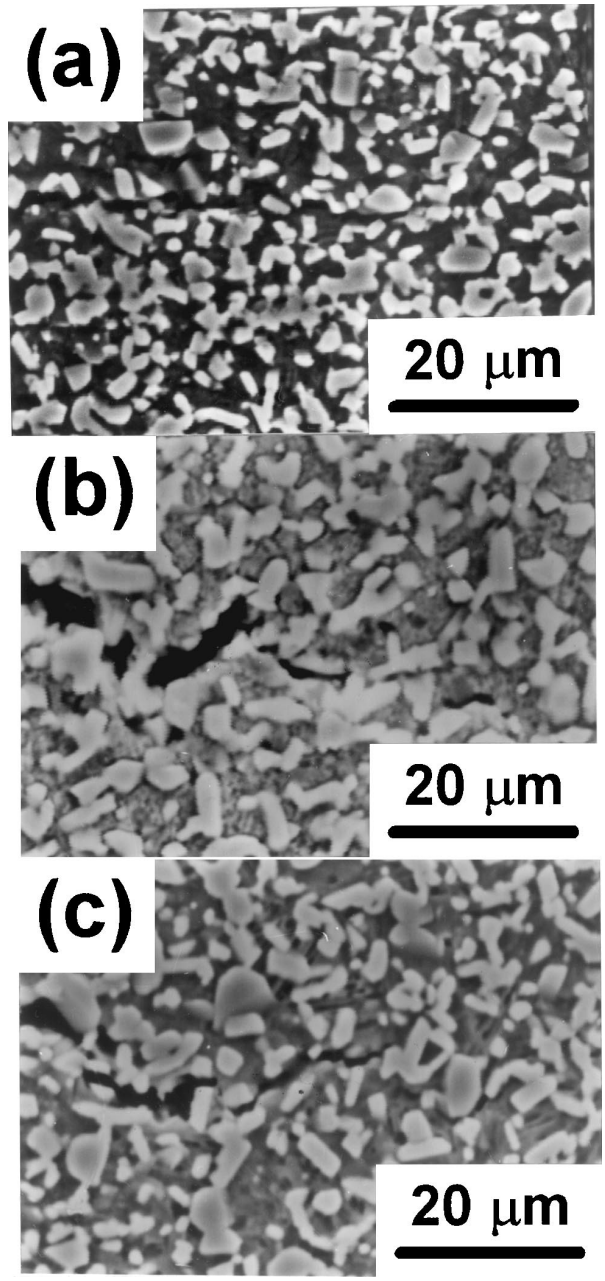

Figure 8 Scanning electron micrographs illustrating crack paths in boride-dispersed composites during fracture toughness testing: (a) HP, (b) ST, and (c) STA.

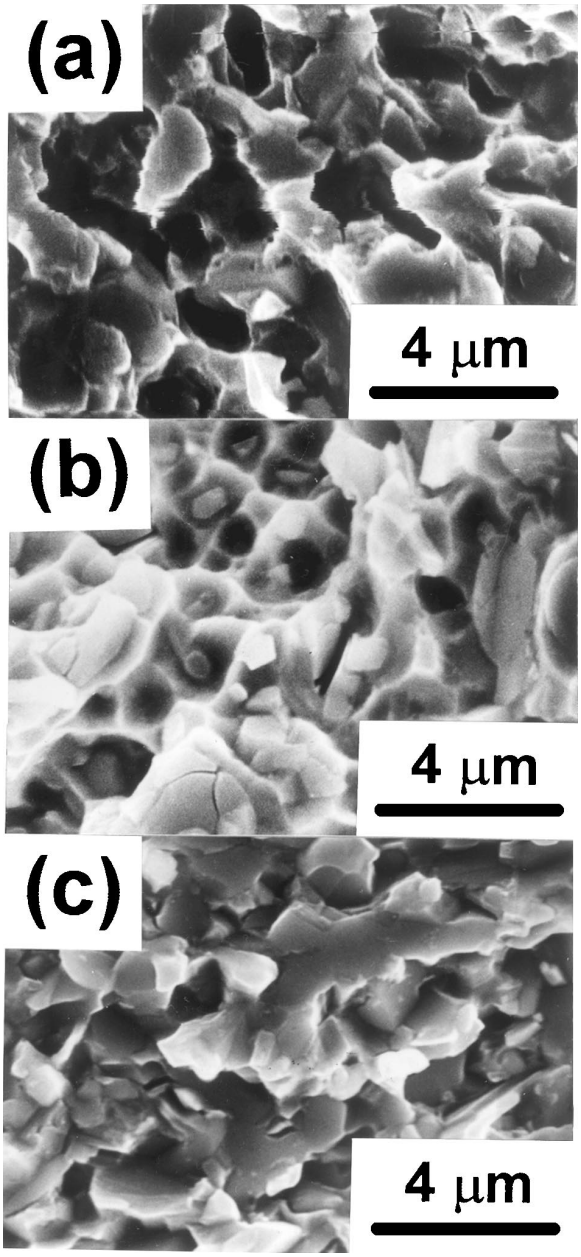

Figure 9 Scanning electron micrographs showing fracture surfaces of boride-dispersed composites after fracture toughness testing: (a) HP, (b) ST, and (c) STA.

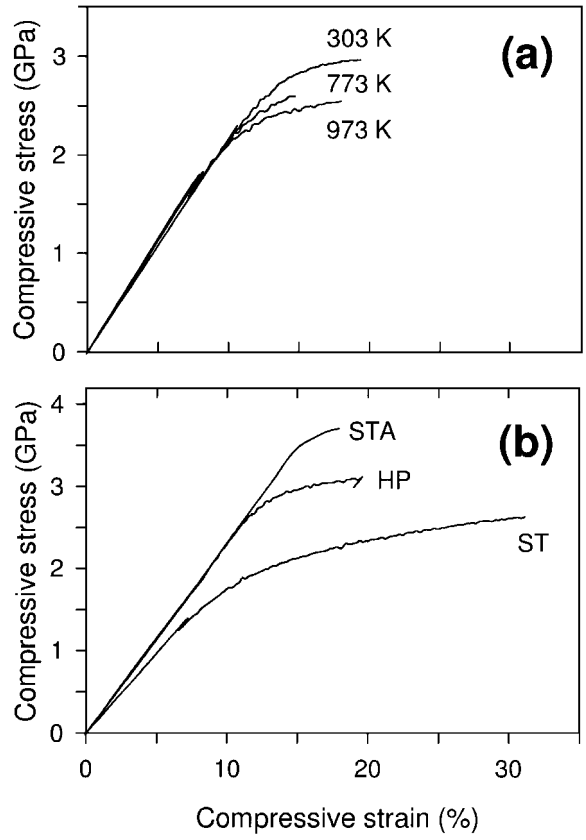

Figure 10 Compressive stress vs. strain for boride-dispersed composites: (a) effect of test temperature on HP material, and (b) HP, ST, and STA specimens tested at 303 K.

References

1. N. MORISHITA, H. KAWATANI, A. SHIMAMOTO, N. KAWAI and T. NIMADE, *Brit. Corros. J.* **26** (1991) 29.
2. T. V. SVISTUNOVA and N. D. SAKUTA, in "Progress in the understanding and prevention of corrosion," edited by J. M. Costa and A. D. Mercer (The Institute of Materials, London, 1993) p. 1285.
3. Y.-R. HE, D. L. DOUGLASS and F. GESMUNDO, *Oxidation of Metals* **37** (1992) 413.
4. H. M. TAWANCY, *Metall. Trans. A* **22A** (1991) 3067.
5. C. R. BROOKS and Y. M. WANG, *Mater. Characterization* **25** (1990) 185.
6. H. M. TAWANCY and N. M. ABBAS, *J. Mater. Sci.* **24** (1989) 1845.
7. C. R. BROOKS, J. E. SPRUIELL and E. E. STANSBURY, *Int. Met. Rev.* **29** (1984) 210.
8. B. CHAKRAVARTI, E. A. STRAKE and B. G. LEFEVRE, *J. Mater. Sci.* **5** (1970) 394.
9. H. M. TAWANCY, *J. Mater. Sci. Lett.* **10** (1991) 696.
10. M. YAMAMOTO, A. SUGIYAMA and H. MATSUSHIMA, *Surf. Sci.* **266** (1992) 322.
11. A. I. TAUB and K.-M. CHANG, in Proceedings of the Seven Sess. Symp. Enhanced Prop. Struct. Met. Rapid. Solidf., edited by F. H. Froes and S. J. Savage (ASM Int., Metals Park, Ohio, United States of America, 1987) p. 437.
12. B. C. GIESSEN, D. E. POLK and R. RAY, United States Patent 4,297,135 (1981).
13. D. RAYBOULD, *Met. Powd. Rep.* **39(May)** (1984) 282.
14. Product data, Consolidated metal products, Allied Corporation.
15. D. RAYBOULD, *The Carbide and Tool Journal* **November/December** (1984) 26.
16. D. RAYBOULD, *Met. Powd. Rep.* **35** (1980) 467.
17. A. NOZUE, M. OTSUKA, H. SUZUKI, M. TAKAYAMA, H. TAGUCHI and T. OKUBO, *J. Japan. Inst. Metals* **58** (1994) 740.
18. S. K. DAS and D. RAYBOULD, in Proceedings of the 5th Conference on Rapid Quenching and Solidification of Metals, Wurzburg, Germany, September 1984, Volume II, edited by S. Steeb and H. Warlimont (Elsevier Science Publishers B. V., Amsterdam, 1985) p. 1787.
19. S. K. DAS, L. A. DAVIS, J. R. WANG and D. KAPOOR, in Proceedings of the 3rd Rapid Solid Processing Conference, National Bureau of Standards, Gaithersburg, MD, December 1982, edited by R. Mehrabian (National Bureau of Standards) p. 559.
20. *Precision Metal* **40(3)** 1982.
21. S.-K. SUH, W.-W. PARK, C.-J. CHOI and Y.-J. PARK, in Proceedings of the 5th International Pacific Conference on Automotive Engineering, Beijing, 1989, p. 360.1.
22. E. J. VINEBURG, E. K. OHRINER, E. P. WHELAN and G. E. STAPLETON, in Proceedings of the TMS/AIME Northeast Regional Meeting on Rapidly Solidified Crystalline Alloys, Morristown, USA, 1985 (TMS/AIME, 1985) p. 1.
23. International Centre for Diffraction Data, Newtown Square, PA, USA.

Received 10 March
and accepted 14 July 1998